ARMY RESEARCH LABORATORY

Evaluation of an Atmospheric Microclimate Model

by Arnold D. Tunick

ARL-TR-1459   November 1997

19971208 031   DTIC QUALITY INSPECTED 2

Army Research Laboratory

Adelphi, MD 20783-1197

ARL-TR-1459   **November 1997**

Evaluation of an Atmospheric Microclimate Model

Arnold D. Tunick
Information Science and Technology Directorate

Abstract

Micrometeorological field data were used in an effort to evaluate an atmospheric microclimate model, specifically, to determine if we can forecast one-dimensional profiles of the atmospheric boundary layer sufficiently well that the corresponding outdoor acoustic field can be reliably calculated.

A soil–plant–atmosphere model was exercised with two sets of experimental data. The model was used to calculate the surface energy budget and to derive meteorological profiles for the overlying boundary layer; both of these were compared to field data. These modeled results were also used to derive outdoor sound-speed profiles and were used as input to a short-range acoustic propagation numerical code.

Contents

Figures

Tables

1. Introduction

In the *Glossary of Meteorology* (Huschke, 1959), "microclimate" is defined as "the fine climate structure of the air space which extends from the very surface of the earth to a height where the effects of the immediate character of the underlying surface no longer can be distinguished from the general local climate (mesoclimate or macroclimate)." In modeling microclimate, one simulates the characteristics of the atmospheric surface and boundary layers. Its time-varying behaviors are related, albeit nonlinearly, to radiative heating and cooling, changes in water content of both the air and soil, terrain, land use, and ground cover. Numerical computer models attempt to simulate the microphysical processes of microclimate for a wide range of applications. In defense technology, microclimate data can be applied operationally, as well as in support of planning, environmental assessment, and research.

Several turbulence-diffusion, atmospheric boundary-layer models are presented in the literature, including those of Avissar et al (1986), Burk (1977, 1980), Blackadar (1978, 1979), Cionco (1965, 1985), Deardorff (1972, 1978), Mellor and Yamada (1974), Naot and Mahrer (1989), Pielke and Mahrer (1975), Yamada and Mellor (1975), and Zhang and Anthes (1982). With some proven measure of accuracy, they attempt to determine the temporal changes of specific meteorological quantities for different environments and sets of initial conditions. Many of these models represent sets of equations for two- and three-dimensional mesoscale (20 to 200 km domain) predictions over complex terrain.

This report documents an evaluation effort in which I studied a one-dimensional (1D) version of the plant-canopy microclimate model, as given by Avissar and Mahrer (1982, 1988), using two dissimilar sets of micrometeorological field data (Clarke et al, 1971; Stenmark and Drury, 1970). I made model calculations of the surface energy budget and compared them to field observations for both data sets. I also computed meteorological profiles for the overlying boundary layer, comparing these also to the observed field data. I used these modeled results to derive outdoor sound-speed profiles. The model output data were also used as input to the acoustic propagation numerical code WSCAFFIP (Noble, 1996; Noble and Marlin, 1995) for calculating levels of short-range acoustic attenuation. My goal was to determine if it was possible to forecast 1D profiles of the atmospheric boundary layer sufficiently well that the corresponding outdoor acoustic field could be reliably calculated. Time-dependent forecasts of microclimate processes are rarely used in atmospheric acoustics (Noble, 1991, 1992).

Following an overview of the soil–plant–atmosphere model (sect. 2), I describe the two evaluation data sets (sect. 3). Model results are discussed in section 4. I then present the derived sound-speed profiles and results from the acoustic propagation numerical code WSCAFFIP (sect. 5). Finally, conclusions are drawn (sect. 6) and recommendations related to this area of study are given (sect. 7).

2. Model Description

The 1D turbulence-diffusion model of the plant-canopy microclimate reported by Avissar and Mahrer (1988) is based on their earlier efforts (Avissar and Mahrer, 1982), as well as the earlier works of Deardorff (1978) and Pielke and Mahrer (1975). It is a simulation model that generates a fairly complex set of calculations at the soil and plant level, so that the surface energy budget (e.g., the transference of heat and moisture) can be made integral to processes within the first 1 to 3 km of the overlying atmosphere. Although the model was originally developed for applications in irrigation management by engineering estimates of actual and potential evapotranspiration (Avissar et al, 1986; Kordova et al, 1994), I revised it to yield time-dependent calculations of the atmospheric acoustic field that result as the derivative of modeled wind speed, wind direction, temperature, and humidity profile estimates.

As initial input, the model requires the numerical equivalent of the day of the year and the time of day (relative to the Greenwich meridian), site location data (latitude and longitude), fraction of sky cloudiness, and ground cover data (i.e., canopy height, leaf area index, surface reflectivity (albedo), thermal emissivity, and aerodynamic roughness length). The model computes soil properties (e.g., hydraulic and thermal conductivity and soil specific heat capacity) from inputs of soil water content, porosity, texture (i.e., proportion of sand, clay, and organic matter), and bulk density. Other model constants include subsoil properties, such as plant root density and distribution. Also, initially, the model requires profile data for air temperature and specific humidity (atmospheric water vapor content) from the ground level to the model top. Lastly, the screen level (2 m above ground level) values of wind speed, wind direction, temperature, and humidity are updated at each hour of the model run.*

The model's estimates of 1D profile structure are computed from a simplified set of kinematic and thermodynamic equations. The transference of momentum (i.e., effects of surface roughness and wind shear) and the exchanges of heat and moisture from one level to the next are calculated in terms of eddy coefficients and vertical gradients that represent the flux. The model turbulence-diffusion equations for momentum can be expressed as

$$\frac{\partial u}{\partial t} = fv - fv_g + \frac{\partial}{\partial z}\left(K_m \frac{\partial u}{\partial z}\right) , \tag{1}$$

$$\frac{\partial v}{\partial t} = -fu + fu_g + \frac{\partial}{\partial z}\left(K_m \frac{\partial v}{\partial z}\right) , \tag{2}$$

for the u- and v-components of wind speed, where f denotes the Coriolis parameter (the deflecting force due to the earth's rotation acting upon

---

Although this model requires a tremendous amount of initial input as well as supporting data for updating calculations every hour, it may still be possible to apply it generally to locations worldwide. One could use bulk estimates of the soil thermal properties and plant or ground cover data, and hourly meteorological inputs (such as wind speed, temperature, or cloud cover) could be extracted from 3D mesoscale model forecasts run independently from the microclimate code.

moving air), the subscript g refers to the geostrophic wind (such that the second terms on the right represent the pressure gradient force), and K_m denotes the exchange coefficient for the diffusion of momentum. In the surface layer K_m is calculated as $K_m = ku_*z/\phi_m$, where k is Karman's constant (a dimensionless constant ($k = 0.4$) of atmospheric fluid dynamics), z is height (in meters), u_* is the friction velocity (in meters per second) that quantifies drag or surface stress, and ϕ_m is the nondimensional wind shear, which accounts for stability, turbulence, and near-ground wind speed profile structure (Monin and Obukhov, 1954; Businger et al, 1971; Dyer, 1974).

In the convective (heated), daytime boundary layer, the model derives the mixing coefficients as a function of height, as suggested by O'Brien (1970). The function can be expressed as

$$K_z = K_{z_i} + \left(\frac{(z_i - z)^2}{(z_i - z_s)^2}\right)\left\{K_{z_s} - K_{z_i} + (z - z_s)\left[\frac{\partial K_{z_s}}{\partial z} + \frac{2(K_{z_s} - K_{z_i})}{z_i - z_s}\right]\right\} , \qquad (3)$$

where z is height above ground level and the subscripts s and i refer to the heights of the top of the surface layer and top of boundary layer, respectively. The profile function K_z is applied similarly for the heat and moisture coefficients where for heat exchange $K_H = k\theta_*z/\phi_H$ and for moisture exchange $K_q = kq_*z/\phi_q$ for $z \leq z_s$, where θ_* and q_* are scaling variables that quantify the near-ground-level gradients (Rachele et al, 1995, 1996a) of temperature and specific humidity, respectively. The model defines $z_s = 0.04 z_i$ and sets $K_{z_i} = 1.0$ for $z \geq z_i$.

Finally, the growth and decay of the planetary boundary layer is calculated from an expression derived by Deardorff (1974), which can be stated as

$$\frac{dz_i}{dt} - w_{z_i} = \frac{1.8\left(w_*^3 + 1.1u_*^3 - 3.3u_*^2 fz_o\right)}{g\frac{z_i^2}{\theta_s}\frac{\partial\theta^\square}{\partial z} + 9w_*^2 + 7.2u_*^2} , \qquad (4)$$

where w_{z_i} is the vertical velocity at z_i (assumed to be negligible or equal to zero, since time-dependent calculations of vertical velocities are not explicitly derived), z_o is the roughness length that characterizes the frictional effects of the land morphology and the type of ground cover, $\partial\theta^\square/\partial z$ is the vertical gradient of potential temperature (pressure scaled temperature) in the stable air immediately above the boundary-layer top, and finally the vertical velocity scaling variable, an implicit calculation of buoyancy, is defined as

$$w_* = \left[(-g/\theta)u_*\theta_*z_i\right]^{1/3} \qquad (5)$$

where g is acceleration due to gravity.

The set of equations for calculations through the soil layer, surface layer, and plant canopy are also given by Avissar and Mahrer (1988). However, in this work I made substitutions based on previous work of Rachele and Tunick (1994) for the equations used to determine solar angles (Woolf, 1968), insolation (Meyers and Dale, 1983), and clouds (Haurwitz, 1945).

The surface energy budget is applied to three layers: the soil (including several thin sublayers); the vegetative canopy and the air throughout the canopy; and the thin (1 to 4 m) layer of air that extends above the canopy top (Avissar et al, 1986). Air temperature and water vapor content for each layer are derived as a result of energy and mass transfers within the system (including plant transpiration). The model also includes heat conduction and moisture diffusion equations for the soil layer, since soil wetness and surface temperature are possibly the two most significant factors determining the partitioning of the total available energy to the soil, evaporative, and sensible heat fluxes. The total available energy (i.e., the net radiative flux) is approximated as a function of transmission, terrain, land use, albedo, canopy leaf area characteristics, soil wetness, and soil thermal properties. The equations of the plant-canopy energy budget are given in table 1.

Table 1. Components of atmospheric surface layer and plant-canopy radiation and energy budget (Avissar and Mahrer, 1988).

Component	Equation	Definition of terms
Plant-canopy energy budget (Carson, 1987)	$R_N = C_H + E_v + S_G$	R_N = net radiative flux C_H = sensible heat flux E_v = evaporation heat flux S_G = soil heat flux
Short-wave radiation (insolation), R_S (Meyers and Dale, 1983)	$R_S = I_o T_R T_G T_W T_A \cos(Z)$	I_o = solar constant ($\approx 1367 \, W/m^{-2}$) T_i = transmission coefficients for Rayleigh scattering (R), absorption by permanent gases (G) and water vapor (W), and scattering due to aerosols (A) Z = solar zenith angle (°)
Sky long-wave radiation, $R_{L\downarrow}$	$R_{L\downarrow} = \sum_{z=0}^{\text{model top}} \left(\varepsilon \sigma T_z^4 \right)$	σ = Stefan-Boltzmann constant ($5.6697 \times 10^{-8} \, W \, m^{-2} K^{-4}$) T_z = air temperature (K) $\varepsilon = \varepsilon_{H_2O} + \varepsilon_{CO_2}$ = total emissivity ε_{H_2O} = emissivity of water vapor ε_{CO_2} = emissivity of carbon dioxide
Net radiation of canopy, R_{NV}	$R_{NV} = \psi_f \left(1 - \alpha_v \right)$ $\left\{ 1 + \alpha_g [1 - \psi_f (1 - t_v)] \right\} R_s + \psi_f \, \varepsilon_v$ $\left\{ [1 + (1 - \psi_f)(1 - \varepsilon_g)] R_{L\downarrow} + \varepsilon_g \sigma T_g^4 \right\}$ $- \varepsilon_v \sigma T_v^4 \left[2 - \varepsilon_v \psi_f^2 (1 - \varepsilon_g) \right]$	ψ_f = shielding factor (full canopy = 1; bare soil = 0) α_v = albedo of plant surface α_g = albedo of soil surface (albedo = reflectivity) t_v = transmissivity of the canopy ε_v = plant foliage emissivity ε_g = soil emissivity T_g = air-ground temperature (K) T_V = canopy virtual temperature that accounts for effects of moisture in air (K)

Table 1. Components of atmospheric surface layer and plant-canopy radiation and energy budget (Avissar and Mahrer, 1988) (cont'd).

Component	Equation	Definition of terms
Net radiation at ground, R_{NG}	$R_{NG} = \left(1 - \alpha_g\right)\left(1 - \psi_f + \psi_f\, t_v\right)R_s$ $+ \left(1 - \psi_f\right)\varepsilon_g\, R_{L\downarrow} + \psi_f\, \varepsilon_g\varepsilon_v\, \sigma\, T_V^4$ $- \varepsilon_g\, \sigma T_g^4\left[1 - \varepsilon_g\, \psi_f\left(1 - \varepsilon_v\right)\right]$	R_s = short-wave radiation, insolation (W/m^2)
Sensible heat, C_H	$C_H = C_{HV} + C_{HG}$	
Sensible heat between canopy and air, C_{HV}	$C_{HV} = \psi_f^* \rho c_p u_* \theta_*$	$\psi_f^* = \dfrac{\text{flux of canopy}}{\text{total flux of canopy} + \text{soil}} = \dfrac{2A_L\psi_f}{1 + 2A_L\psi_f}$ A_L = leaf area index
Sensible heat between ground and air, C_{HG}	$C_{HG} = \left(1 - \psi_f^*\right)\rho c_p u_* \theta_*$	ρ = density of air (kg/m^3) c_p = specific heat of air (J/kgK) u_* = surface friction velocity (m/s) θ_* = surface scaling temperature (K)
Evaporation flux, E_V	$E_V = E_{VV} + E_{VG}$	
Evaporation flux between canopy and air, E_{VV}	$E_{VV} = \psi_f^* \rho L^* u_* q_*$	L^* = heat of vaporization or condensation (J/kg) q_* = surface scaling specific humidity (g/g)
Evaporation flux between ground and air, E_{VG}	$E_{VG} = \left(1 - \psi_f^*\right)\rho L^* u_* q_*$	
Soil heat flux, S_G	$S_G = -\lambda \dfrac{\partial T_g}{\partial z}$	λ = soil thermal conductivity (W m^{-1}K^{-1}; derived in terms of soil composition and soil wetness)
Heat conduction	$c_s \rho_s \dfrac{\partial T_g}{\partial t} = \dfrac{\partial}{\partial z}\left[\lambda \dfrac{\partial T_g}{\partial z}\right]$	c_s = soil specific heat (J m^{-3} K^{-1}) ρ_s = soil density (kg m^{-3})
Soil moisture diffusion (Naot and Mahrer, 1989)	$\dfrac{\partial \Delta}{\partial t} = \dfrac{\partial}{\partial z}\left[D_\Delta \dfrac{\partial \Delta}{\partial z}\right] + \dfrac{\partial}{\partial z}\left[D_T \dfrac{\partial T_g}{\partial z}\right]$ $+ \dfrac{\partial K_h}{\partial z} - L_{PT}$	Δ = soil water content (%) D_Δ = isothermal moisture diffusivity D_T = thermal moisture diffusivity K_h = hydraulic conductivity (m/s) L_{PT} = soil water loss through plant transpiration

3. Field Data

3.1   Hay 1967

One of the sets of experimental data used in this study was collected during a field campaign near the town of Hay, New South Wales, Australia (34.50, 144.93), which took place during the 1967 southern hemisphere winter, from 15 July to 27 August (Clarke et al, 1971). This very large data set was collected over an extensive flat area (3600 km^2), where the ground cover was predominantly sparse low vegetation over dry soil. For the task at hand (model verification with regard to surface-layer and overlying boundary-layer profile structure), the data were highly suitable in all areas except for plant-canopy interactions. Five types of surface-layer and mixed-layer data were collected: (1) hourly 16-m micrometeorological tower measurements of wind speed, specific humidity, and temperature; (2) hourly surface measurements of the net radiative balance and soil heat flux; (3) measurements of wind speed and wind direction from 0 to 2 km (AGL—above ground level) obtained by hourly pibal (pilot balloon) flights; (4) measurements of pressure, temperature, and mixing ratio (m_r = mass$_{water\ vapor}$/mass$_{dry\ air}$), to a height of 2 km, taken by radiosonde (instrumented balloon sonde) flights at 3-hr intervals; and (5) reports of fractional, low, high, and total cloud cover (including cloud type descriptors).

Of the 1050 hourly reports (profiles) of published observations, I used those collected during the 27-hr period from 2100 LT (local time) on 15 August 1967 to 2400 LT on 16 August 1967. This data-collection period was characterized by clear skies and relatively light daytime wind speeds. Dry soil promoted strong surface-based convective heating. The soils for the field area were predominantly brown loams overlying red-brown clay subsoils.

3.2   Davis 1966

The second set of experimental data used in this study was collected during a field study at Davis, California (38.33, 121.44), during the summer of 1966 and spring 1967 (Stenmark and Drury, 1970). The field site was a flat, fescue-grass-covered 50,000-m^2 area at 17-m elevation (above mean sea level). It was about 2 km west of the main portion of the University of California at Davis campus, 113 km northeast of San Francisco. The data were taken during periods when fields surrounding the test area were for the most part crop covered and well irrigated, giving (in effect) horizontal uniformity to the surface conditions with respect to temperature and moisture. Advection effects due to the site's proximity to the coast were considered to be negligible during the data-collection period. Profiles of wind speed, temperature, and specific humidity were taken at nine levels from 25 to 600 cm. In addition, infrared radiometers, ground heat flux plates, and a large (3.0-m-diameter) weighing lysimeter were used to record the net radiation, the soil heat flux, and surface evaporation rates, respectively. The energy budget equation was used to determine the sensible heat flux

C_H as the residual. The soils at the Davis field site were predominantly silt loams.

In the present study, I used the 30-hr subset of data taken from 0100 LT on 13 July 1966 to 0600 LT on 14 July 1966. This data interval was characterized by clear skies, damp soil, low wind speeds through the morning, and moderate wind speeds through the afternoon. Increased evaporation rates associated with the change (increase) in surface wind speeds were observed. (The surface wind direction (190° to 210°) remained, for the most part, constant.) The data collected from this site were very well suited for verifying the model with regard to surface-layer energy budget calculations.

3.3   Model Parameters from Data Sets

Table 2 gives model parameters for both the Davis 1966 and Hay 1967 data sets. Typical values given for albedo and surface roughness for other combinations of soils and ground cover can be retrieved from Hansen (1993a, 1993b). Hourly meteorological input for both data sets is given in tables 3 and 4.

Table 2. Model parameters for Hay 1967 and Davis 1966 data sets.

Variable name	15–16 August 1967 Hay, Australia	13–14 July 1966 Davis, CA
Latitude	34.50 S	38.33 N
Longitude	144.93 E	121.44 W
Albedo	0.20	0.27
Emissivity	0.98	0.96
Roughness length	0.13 cm	1.40 cm
Ground cover/canopy height	barren field/0.0 cm	dense field/10.0 cm
Leaf area index	0.0	1.0
Soil properties:		
Water content	0.08 %	0.20 %
Thermal conductivity	0.539 W m^{-1} K^{-1}	0.947 W m^{-1} K^{-1}
Volumetric specific heat	1.374 J m^{-3} K^{-1}	1.887 J m^{-3} K^{-1}
Density	1400.0 kg m^{-3}	≈1400.0 kg m^{-3}
Soil texture:		
% sand	28.0	20.0
% clay	70.0	77.0
% organic	2.0	3.0

Table 3. Meteorological model input (1-hr average data) for Hay 15–16 August 1967 data set (winter).	Local time	Temperature (°C)	Specific humidity (g/kg)	Wind speed (m/s)	Wind direction (°N)
	21	5.4	4.818	1.75	165
	22	4.0	4.266	1.67	155
	23	3.3	4.295	1.39	156
	24	2.8	4.190	1.57	160
	1	2.2	4.058	1.71	160
	2	2.2	4.058	2.18	162
	3	1.7	3.957	2.03	159
	4	0.6	3.693	1.67	159
	5	−0.3	3.495	0.77	158
	6	−0.3	3.531	0.40	155
	7	−0.4	3.506	0.40	142
	8	0.9	3.774	1.21	138
	9	5.3	4.893	2.71	107
	10	9.2	5.768	2.41	89
	11	11.7	6.241	2.23	113
	12	12.7	6.311	2.62	102
	13	13.3	6.380	1.90	116
	14	13.8	6.401	2.91	127
	15	14.2	6.472	2.85	108
	16	14.6	6.543	3.62	111
	17	14.6	6.440	3.04	94
	18	12.3	6.057	1.61	105
	19	8.1	5.217	2.06	119
	20	6.5	4.848	1.64	120
	21	5.6	4.664	1.79	111
	22	4.3	4.256	1.39	104
	23	2.8	4.008	1.80	103
	24	2.6	3.951	1.81	98

Table 4.	Local time	Temperature (°C)	Specific humidity (g/kg)	Wind speed (m/s)	Wind direction (°N)
Meteorological model input (30-min average data) for Davis 13–14 July 1966 data set (summer).	1	12.81	8.08	1.800	154
	2	12.46	8.03	1.839	146
	3	12.08	7.96	1.239	167
	4	11.96	7.92	0.313	167
	5	11.46	7.69	0.516	145
	6	12.74	8.14	1.648	299
	7	15.03	8.48	1.934	327
	8	17.21	9.12	1.845	336
	9	19.21	9.63	1.629	276
	10	20.63	10.11	1.939	194
	11	22.61	10.22	1.408	210
	12	23.88	10.11	2.865	218
	13	25.12	9.92	3.247	208
	14	25.85	9.33	5.026	192
	15	25.84	8.67	5.932	206
	16	25.12	8.24	5.738	218
	17	23.40	8.16	5.429	210
	18	21.87	8.10	5.151	204
	19	18.85	7.72	4.403	206
	20	16.48	7.30	4.582	210
	21	14.46	7.47	3.177	208
	22	13.50	7.46	2.723	204
	23	13.19	7.50	3.686	205
	24	12.82	7.49	3.996	210
	1	12.43	7.67	3.966	204
	2	11.87	7.47	3.739	198
	3	11.68	7.44	3.432	200
	4	11.51	7.35	3.979	192
	5	11.34	7.27	2.923	194
	6	12.56	7.6	1.902	240

4. Model Results

4.1 Surface Energy Budget

Figure 1 shows computations for two components of the surface energy budget (net radiation and soil heat flux) for the Hay data set, along with field data. The calculated and observed data appear well matched. As these results show, the model is generally effective in computing radiative exchanges over near-barren ground and heat transfer through a dry soil layer.

On the other hand, ground temperature approximations (not shown) were somewhat underestimated, as much as 1 to 3 °C, particularly during the night and early morning hours before sunrise. Had the predicted surface temperatures been more in line with the observed data for those times, the calculated value for the outgoing soil flux would have been higher. Often, discrepancies of this kind between data and model output can be minimized by a process of iterative "tuning" (i.e., adjustments made within justifiable limits) of just a few specific input parameters, such as soil water content, albedo, or surface roughness, for example. In this case, however, the model was relatively unresponsive to this kind of tuning.

Figure 2 shows estimates of the surface energy budget for the Davis 1967 data set. The model calculations agree remarkably well with the observed data for the net radiative flux and the evaporative flux above the irrigated canopy layer. The sensible heat and soil heat fluxes, however, do not agree as well with the observed data as would have been expected considering the other computed results. In previous work with this data set (Rachele and Tunick, 1994; Rachele et al, 1996b), it was found that increased wind speeds beginning from 1300 to 1400 LT (see table 4) were catalysts for higher rates of evaporation, drawing heat from the air in the layer adjacent to the canopy, and promoting increased surface layer stability. In the model calculations reported here, however, the sensible cooling of the air did not seem to take place as I would have expected. Figure 2 shows a nearly 3-hr time difference where $C_H = 0.0$ W/m^2. The modeled excesses in the sensible heat flux suggests that the calculated surface temperatures (not shown) may have been too high. These surface layer processes, by the
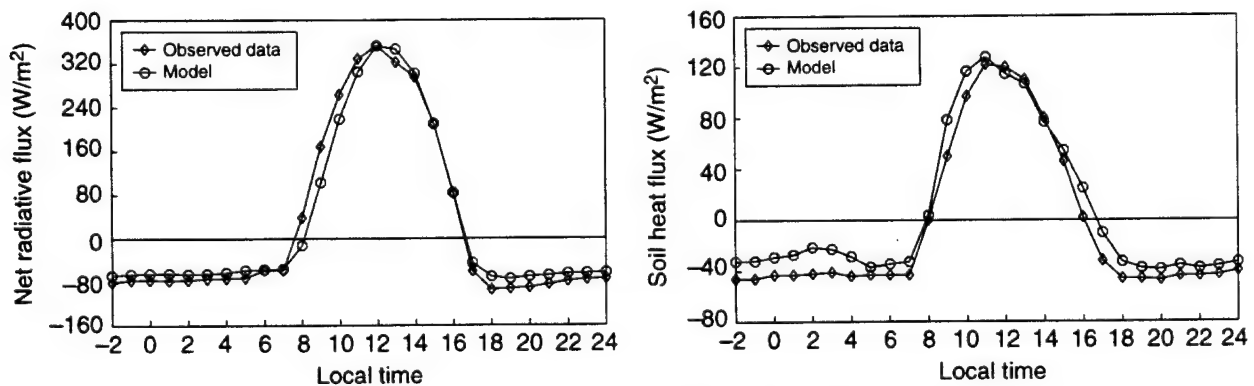

Figure 1. Model comparisons to observations of net radiative flux (left) and soil heat flux (right) for Hay 1967 data set.
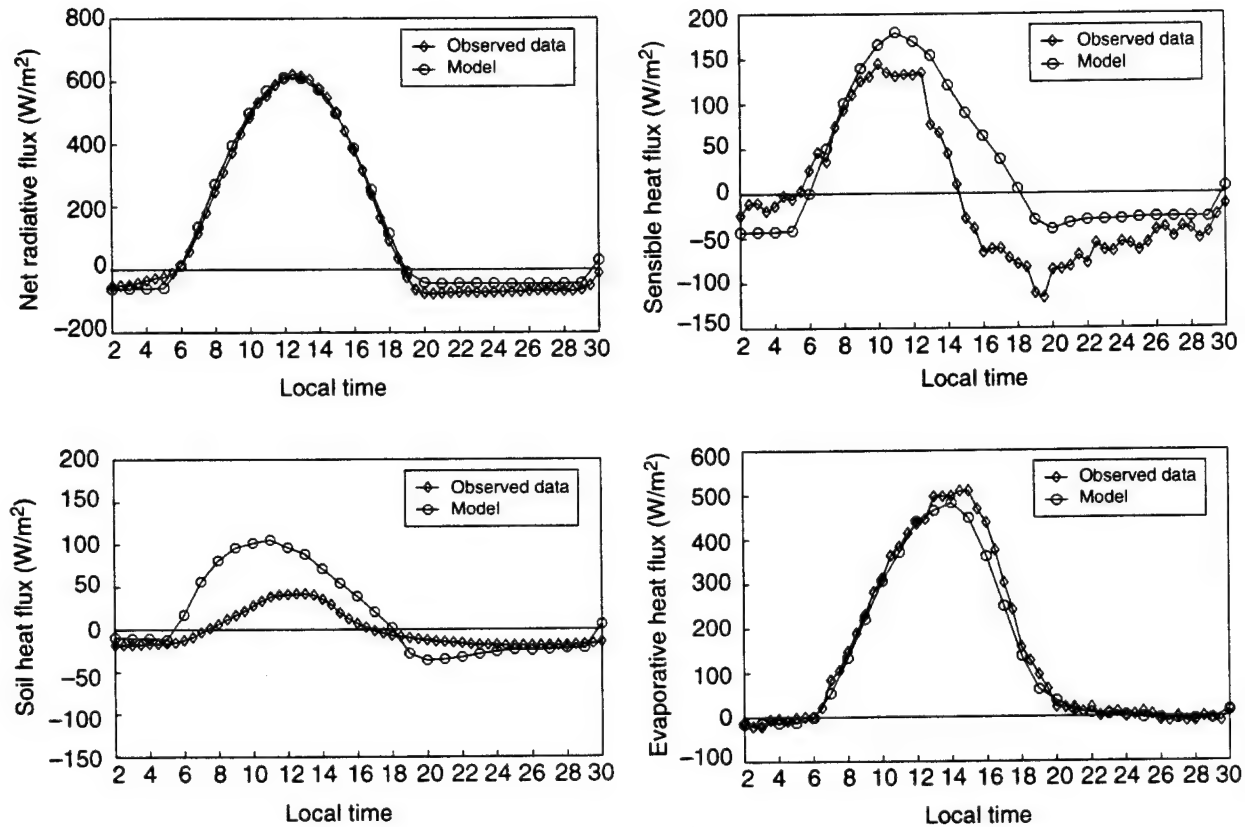
Figure 2. Model comparisons to observations of net radiative flux (top left), sensible heat flux (top right), soil heat flux (bottom left), and evaporative heat flux (bottom right) for Davis 1966 data set.

definition of microclimate, affect the structure of temperature, wind speed, and humidity profiles through the overlying boundary layer (as I show in sect. 4.2).

4.2 Boundary-Layer Profile Structure

From the boundary-layer data collected at Hay, I studied 6- and 18-hr forecasts in order to evaluate the microclimate model with regard to mixed layer profile structure. Figure 3 shows modeled and recorded air temperature and specific humidity profiles. The model output agrees with many of the gross features of the observed data: for example, the simulated nighttime temperature inversions (top left) appear to be captured by the model, even though the intensities of the near-surface and upper-level gradients differ. The computed temperature profiles for the daytime case (top right) also appear to be in agreement with observed data; however, the temperature profile gradients at the top of the boundary layer are clearly offset (see fig. 4). On close inspection, the model and observed daytime temperature surface gradients are offset as well.

As a matter of convention, for the net radiative and soil heat flux, positive values represent energy transferred downward, while negative values represent energy transferred away from the soil–plant–atmosphere interface. The opposite is an accepted convention for the sensible and evaporative heat fluxes.
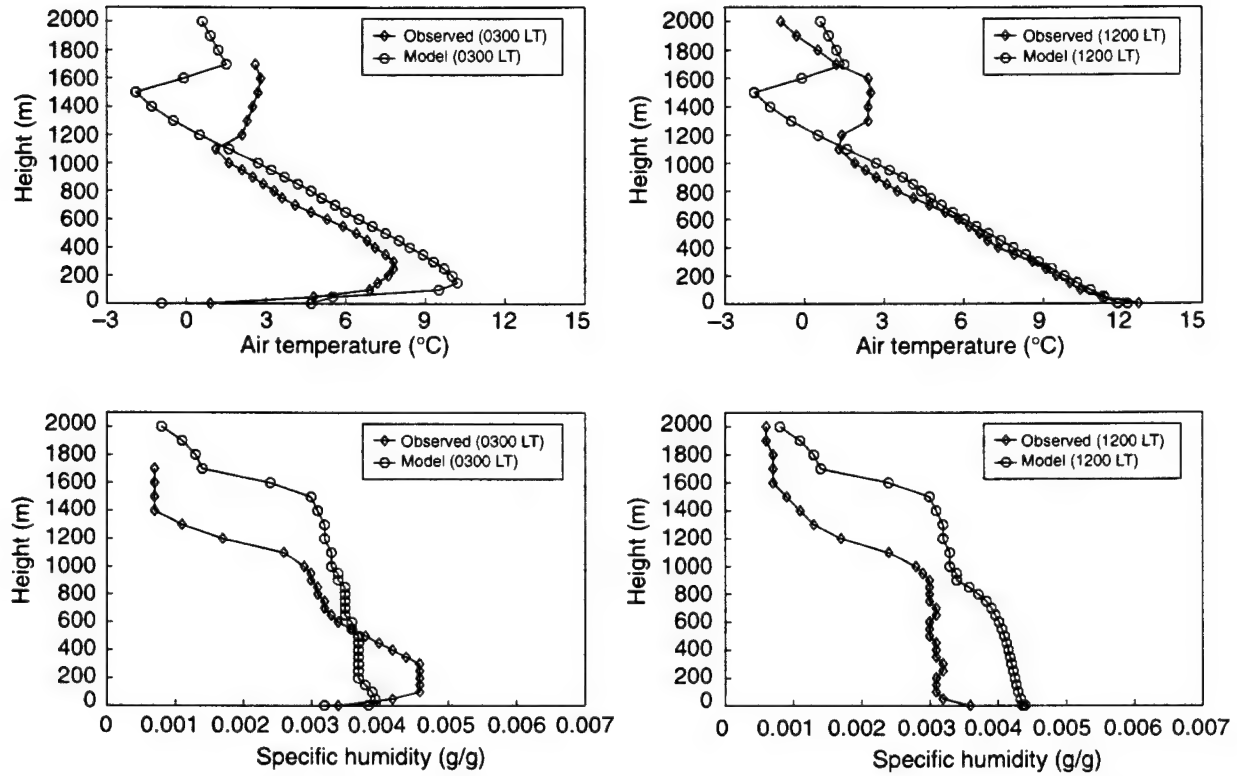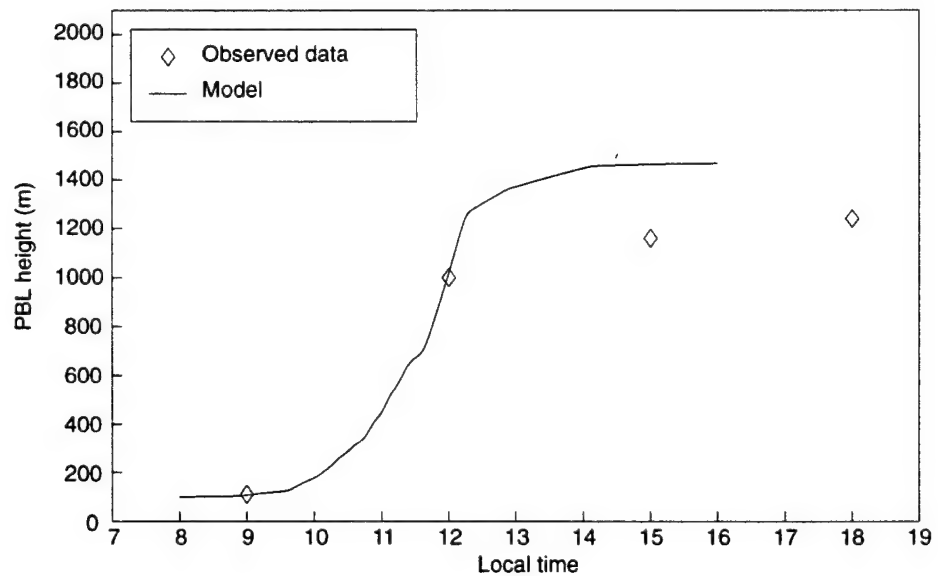
Figure 3. Model comparisons to observations of profiles of boundary-layer temperature (top) and specific humidity (bottom) for Hay 1967 data set.

Figure 4. Model comparison to observations of depth of planetary boundary layer for Hay 1967 data set.

The simulated specific humidity profiles in figure 3 (bottom) show offsets in water vapor content through the upper and lower levels of the boundary layer, in contrast to the observed data. The observed data indicate a characteristic drying out of the lower atmosphere due to vertical mixing. Alternatively, the modeled profiles indicate tendencies toward an overall increase of boundary layer moisture over this period of time.

By definition, mixing depths are determined as a function of boundary-layer growth and decay. These processes, in general, are driven by the radiative exchanges that govern the surface heat and moisture budget. Therefore, discrepancies between predicted and observed inversion heights are most often due to the inaccuracy of the predicted surface-layer gradients. Otherwise influences on boundary-layer growth must be attributed to external and upper-level forcings, such as advection or changes in the large-scale horizontal pressure gradient. The unmatched inversions shown in figure 3 are then most likely the result of overpredicted surface-layer heating. This was found to be the case in an earlier study that was repeated by Pielke and Mahrer (1975) using the prediction expression of Deardorff (1974) (eq (4), sect. 2, this report). Values of calculated mixed-layer heights, shown in figure 4, compared to those determined from observations are given in table 5.

Figure 5 shows model-derived wind speed and wind direction. The 1D model predicts an observed, nighttime wind speed maximum (left) very poorly. It also fails to match fluctuations in the observed daytime wind speed profile (right) although on average, the mean differences are less than 1 m/s.

Diurnal accelerations and decelerations in wind speed are normally due to changes in mesoscale pressure gradients (over a range of 20 to 200 km). These gradient changes are brought about by changes in temperature near the ground, which increase or decrease aerodynamic drag and stress (McNider and Pielke, 1981). To model these processes adequately, one would need time-dependent, 3D, horizontal and vertical transfer equations for momentum, mass, and temperature for each point in a user-defined grid. From the results of this study, it becomes apparent that the 1D approach is not sufficient.

The forecasts of wind direction profile structure shown in figure 5 (bottom) are also poor through the forecast period, even though mean differences may appear to be on the order of ±15°. It is known that wind directions are probably the most difficult variable for meteorological simulation models

Table 5. Calculated heights of planetary boundary layer compared to observations.

	Height of boundary layer (m)	
Local time	Observed data[a]	Model
0800	—	100.00
0900	110.00	107.36
1000	—	175.20
1100	—	439.79
1200	1000.00	1018.05
1300	—	1373.03
1400	—	1448.27
1500	1160.00	1464.05
1600	—	1468.23
1700	—	100.00
1800	1240.00	100.00

[a]Estimated from observed potential temperature and specific humidity profile data (Pielke and Mahrer, 1975).

to predict. Events on a number of different scales, from frontal passages to local urban or rural land use, affect wind direction. Assessments of predicted wind direction have shown tremendous scatter compared to observations (see fig. 13.2 in Gross, 1994). However, next to temperature and changes in temperature with height, wind speed and direction are significantly important in assessing the outdoor acoustic field that results as a derivative of a microclimate forecast. The last sections of this report discuss the assessment of outdoor acoustic fields in greater detail.
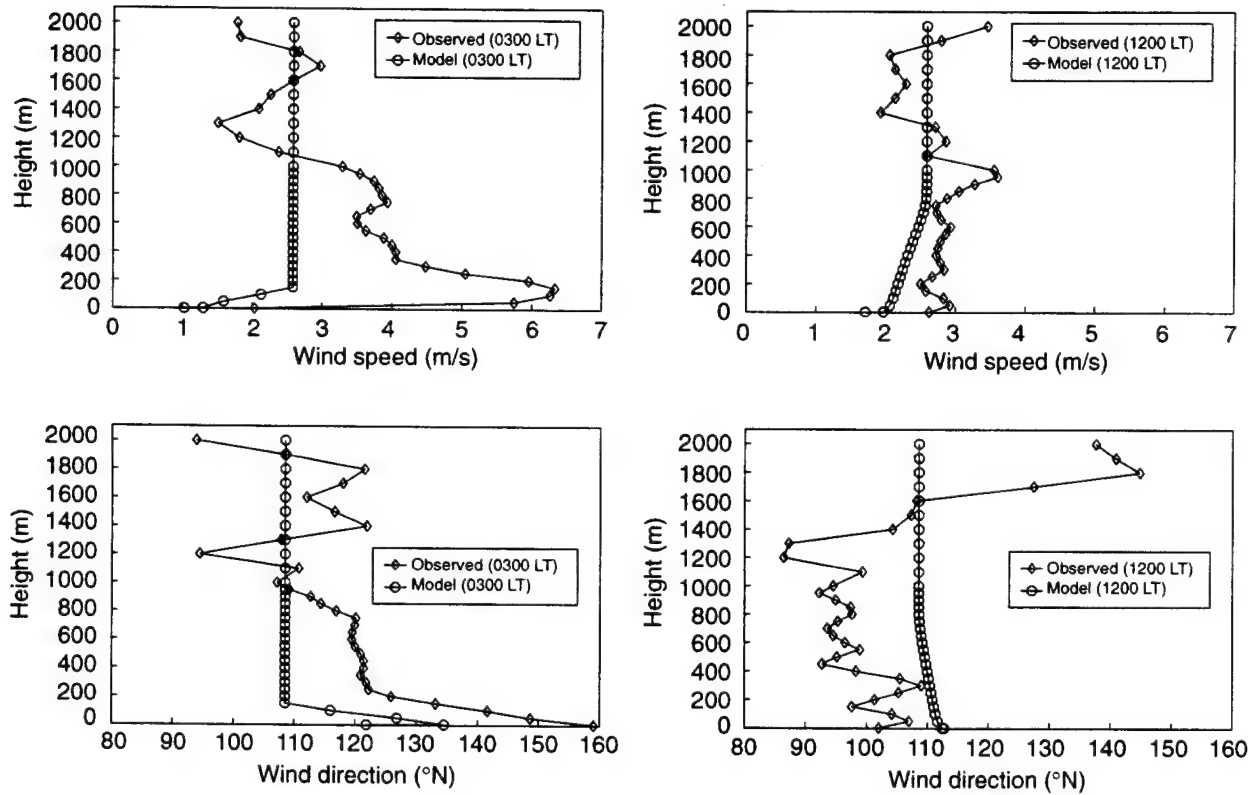
Figure 5. Model comparisons to observations of profiles of boundary-layer wind speed (top) and wind direction (bottom) for Hay 1967 data set.

14

5. Application to Atmospheric Acoustics

5.1 Calculated Boundary-Layer Sound-Speed Profiles

First-order approximations of sound speed in the absence of wind can be derived from the expression in Pierce (1981) given as

$$C(T) = \sqrt{\frac{\gamma R T}{M}} \; , \tag{6}$$

where γ is the ratio of the specific heats of air for constant pressure and constant volume modified to account for water vapor content so that $\gamma = (7 + h)/(5 + h)$, where h is the fraction of water molecules in the air, R is the universal gas constant ($8314.16 \text{ kg}^{-1} \text{ K}^{-1}$), T is air temperature in kelvins, and M is molecular weight, calculated as $M = 29 - 11h$. However, the variations of sound speed caused by even extreme changes in humidity are minimal (approximately 1 to 2 m/s) and can generally be ignored (Noble and Marlin, 1995). The effect of winds on sound speed is expressed by a vector relation. Equation (6) can be rewritten as

$$C_{eff}(z) = C(T) + U \cos (\theta_w - \pi - \theta_R) \; . \tag{7}$$

where $C(T)$ is the sound speed in the absence of wind at temperature T, U is the mean horizontal wind speed (in meters per second), θ_w is the wind direction (conventionally interpreted as the direction from which the wind originates), $\theta_w - \pi$ is interpreted as the along-wind direction, and θ_R is the azimuth or bearing of an outlying receiver from a given acoustic source. The environmental effects on the propagation of acoustic energy, as reviewed by Noble (1992), are related to the height-dependent variations of the sound-speed profile, which, in general, cause (1) upward refracting conditions, when the sound-speed gradients through the first 0 to 400 m of the mixed layer are negative (normally occurring during the day), or (2) downward refracting conditions, when the sound-speed gradients are positive (normally occurring at night).

Figure 6 shows the derived boundary-layer sound-speed profiles for the nighttime and daytime cases. There appears to be reasonably good agreement between the sound-speed profiles derived from model calculations and those derived from the field data, particularly for the daytime case shown. Differences between the results are principally related to the combined accuracy of simulated gradients in temperature and wind-speed profile structure. (It is only by a matter of convention that the calculations in the bearing $\theta_{surface}$ (left) are called upwind, while those made in the bearing $\theta_{surface} - 180°$ (right) are called downwind.)

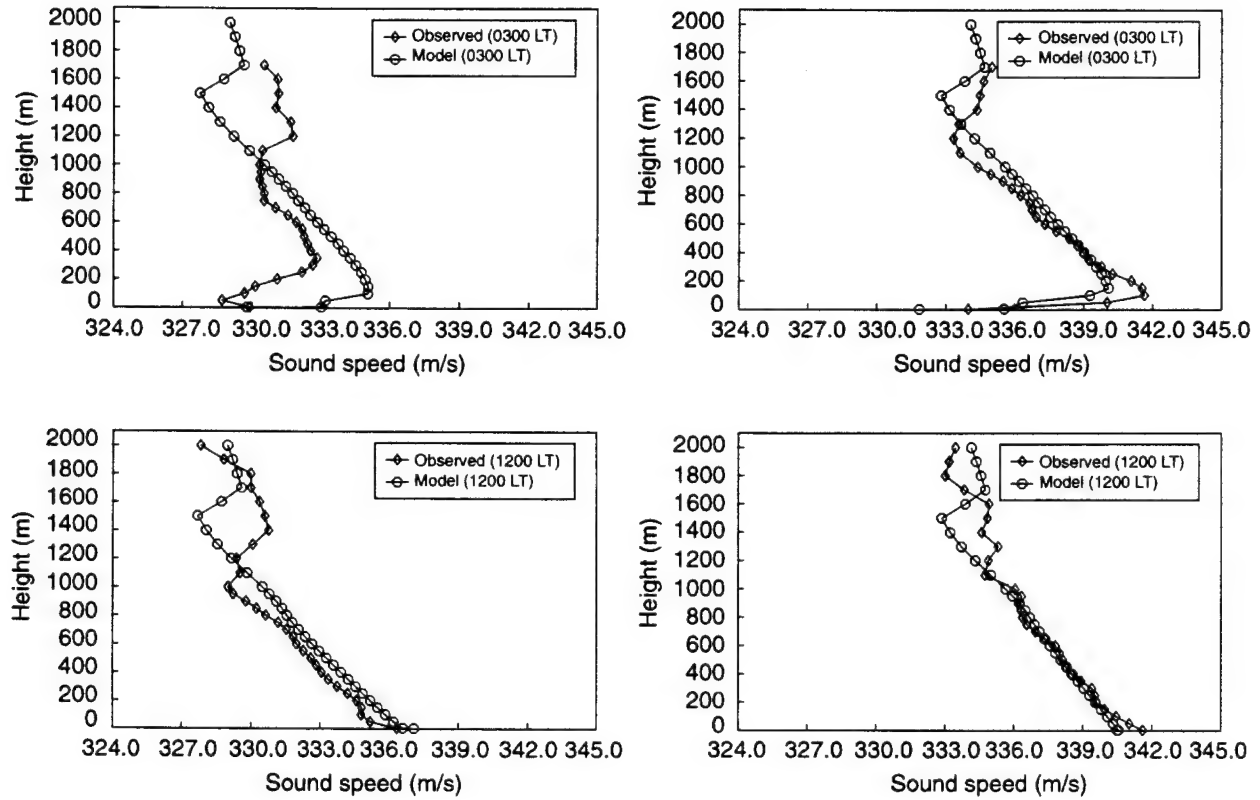**Figure 6. Derived boundary-layer sound-speed profiles for nighttime (top) and daytime (bottom) atmospheric conditions.**

## 5.2   Approximations of Short-Range Outdoor Acoustic Attenuation

Meteorological profiles from observed Hay field data and those forecast by the model in this study were used as input to the acoustic propagation numerical code WSCAFFIP (Windows (version) Scanning Fast Field Program), which assesses environmental effects on short-range acoustic attenuation. WSCAFFIP provides attenuation levels with range and azimuth for a given geometry and frequency (Noble, 1996; Noble and Marlin, 1995). The acoustic propagation algorithms in WSCAFFIP attempt to represent the effects of atmospheric refraction, diffraction, absorption, and reflection or ground impedance. Figure 7 shows the WSCAFFIP results for the upwind (top) and downwind (bottom) nighttime cases. Ahead of the first segment of the data (i.e., $x \leq 650$ m), the calculated attenuation levels appear to be well matched. Further out in range, differences in the derived sound-speed profile gradients have resulted in either sound-limited areas (shadow regions) or areas of refocusing due to refraction (i.e., the local minima and maxima). As a rule, the more positive the sound-speed gradient (see fig. 6 (top)), the greater the effects of a downward refracting atmosphere, especially in the case of calculations made in the downward direction.

Figure 7. Short-range acoustic attenuation upwind (top) and downwind (bottom) predicted by WSCAFFIP numerical code for nighttime atmospheric conditions.
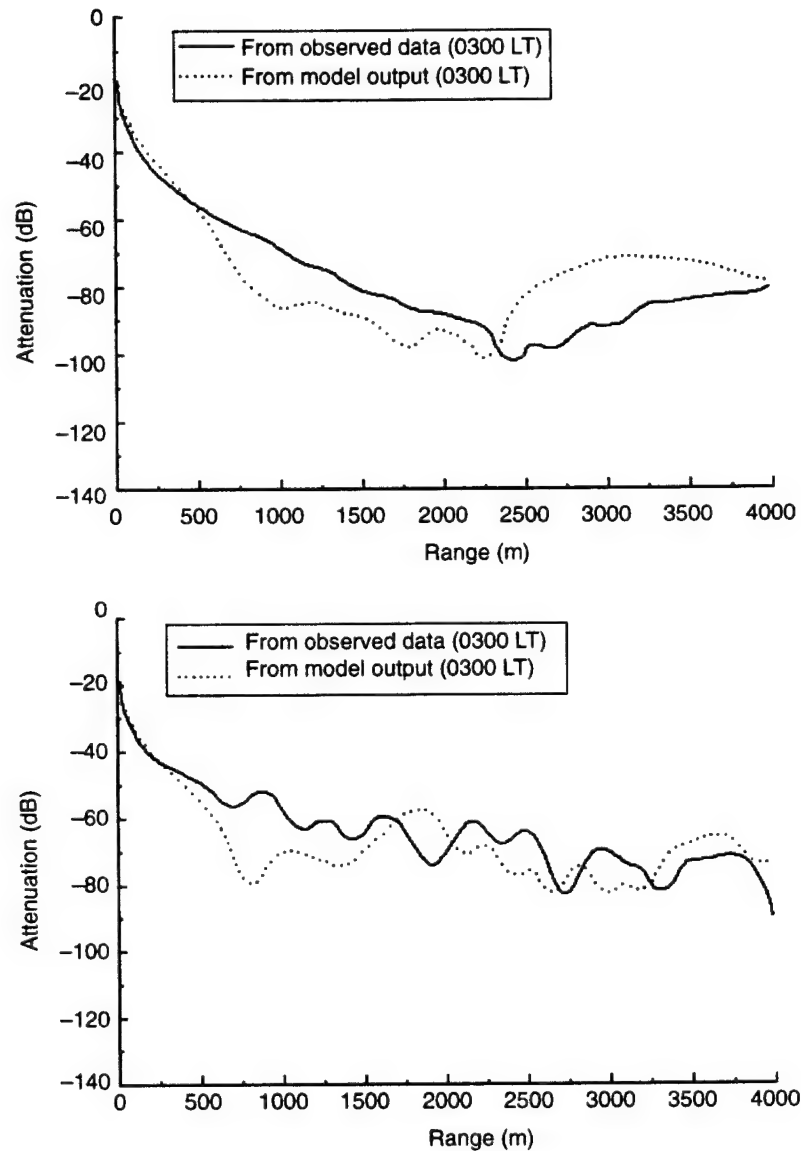
In contrast, the attenuation levels for the daytime case (fig. 8) show the effects of upward refracting atmospheric conditions. The amount of attenuation appears to be, overall, greater than in the nighttime case. Sound levels are shown to be in good agreement to a distance of approximately 1750 m in range. Beyond 1750 m, offsets in the profiles predictions have affected the degree of separation in the data, as seen in both figures in the range from 2000 to 4000 m.

Figure 8. Short-range acoustic attenuation upwind (top) and downwind (bottom) predicted by WSCAFFIP numerical code for daytime atmospheric conditions.
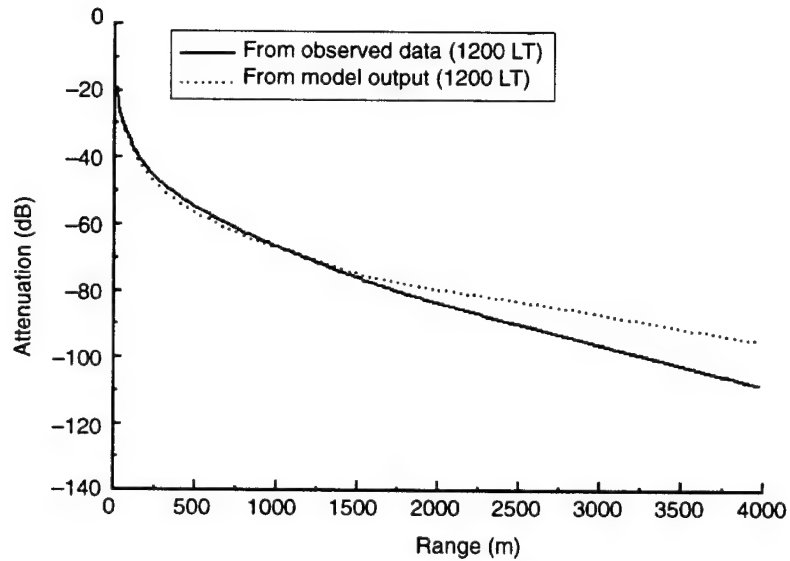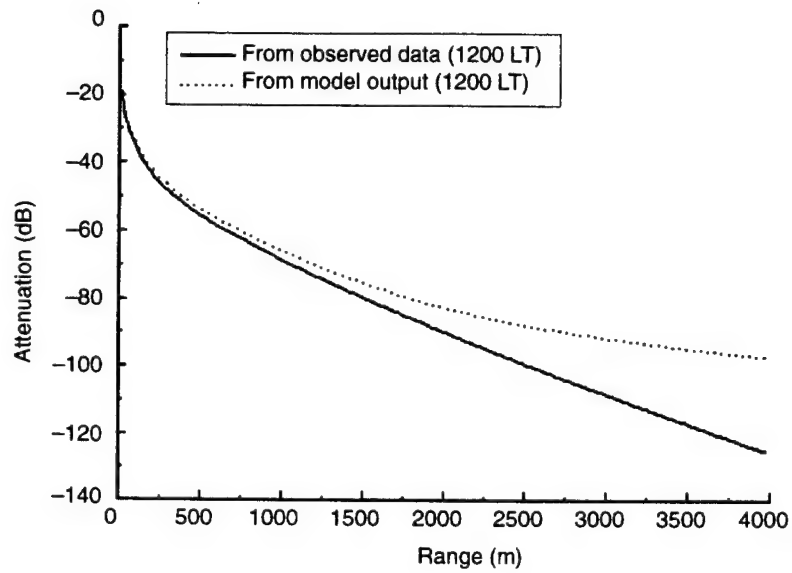
6. Conclusions

In the work reported here, I used micrometeorological field data in an effort to evaluate an atmospheric microclimate model. I set out to determine if it was possible to forecast 1D profiles of the atmospheric boundary layer sufficiently well that the corresponding outdoor acoustic field could be reliably calculated.

Specifically, I studied a soil–plant–atmosphere model using two dissimilar sets of experimental data: Hay 1967 and Davis 1966. Model calculations of the surface energy budget were compared to field observations. Derived meteorological profiles for the overlying boundary layer were also compared to data. Using these modeled results, I derived outdoor sound-speed profiles. I also used the modeled results as input to the short-range acoustic propagation numerical code WSCAFFIP.

Some general conclusions with regard to the evaluation of this atmospheric microclimate model follow.

1. Quantitative assessments of the surface energy budget over land principally rely upon equations sensitive to variations in soil wetness and surface temperature, since these are probably the two factors most significant determining the partitioning of the soil, evaporative, and sensible heat fluxes.

2. As shown by the results of the surface energy budget calculations with the Hay 1967 field data used as input, the model is, overall, effective in computing radiative exchanges over sparsely covered ground and heat transfer through a dry soil layer.

3. Discrepancies between data and model output can normally be minimized by a process of iterative "tuning" of just a few specific input parameters, such as soil water content, albedo, or surface roughness. For the case with the Davis 1966 data used as input, however, the model was relatively unresponsive to this kind of tuning. Therefore, although the radiative and evaporation flux calculations for the irrigated canopy were in good agreement with the field data, the sensible and soil heat fluxes agreed less well with the observed data than I had expected.

4. The 1D forecasts of meteorological profile structure in the atmospheric boundary layer were generally very poor, especially with regard to windspeed. This level of model performance was disappointing. The 1D approach appears to be insufficient to effectively represent effects of surface roughness, wind shear, and the exchanges of heat and moisture from one level to the next.

5. Quantitative assessments of the outdoor acoustic field rely upon accurate representations of the local meteorology, since variations in the profile gradients of sound speed are determined from these data. Therefore, the discrepancies in the forecasts of short-range acoustic attenuation with range presented in this study were most likely due to sufficiently significant offsets in the profiles of sound speed, particularly in the 0 to 400 m layer above ground.

19

7. Recommendations

The components of the atmospheric surface energy budget, by definition, reflect the rates of heating and cooling near the ground. The transfer of incident, reflected, and emitted energy at the surface can be approximated as functions of cloud cover, terrain roughness characteristics, surface albedo, canopy leaf area, soil water, and soil thermal capacities. As an integral part of the microclimate, the surface energy budget acts as the principal influence on the development of pressure, temperature, and humidity gradients on all scales. As a result, most of the turbulence and diffusion of heat, momentum, and moisture in the boundary layer can be attributed to surface layer energy exchanges. They are inherently multidimensional processes.

In recent years, however, several efforts have relied on 1D meteorology for defense-related applications, in particular, outdoor acoustics. Both models and measured field data have been manipulated in efforts to create reliable product codes. Unfortunately, at the conclusion of each initiative, it is found that better assessments or forecasts of wind, temperature, and humidity fields require further research (into models that can account for changes in the state variables over time, both horizontally and vertically, from within as well as from outside the modeling area of interest). The 1D approach applied to areas 10 to 80 km across has been insufficient, especially with regard to estimates of wind speed and wind direction. In application, only limited successes have been realized. Therefore, because of their explicit dependence on temperature and wind profile structure, acoustic attenuation models, especially, need to incorporate 3D meteorological data (or forecast fields). Their reliability in the battlefield environment would then, in my opinion, greatly improve.

References

Avissar, R., and Y. Mahrer, 1982: "Verification Study of a Numerical Greenhouse Microclimate Model," *Trans. Amer. Soc. Agric. Eng.* **25**, 1711–1720.

Avissar, R., and Y. Mahrer, 1988: "Mapping Frost-Sensitive Areas with a Three-Dimensional Local-Scale Numerical Model. Part I: Physical and Numerical Aspects," *J. Appl. Meteorol.* **27**, 400–413.

Avissar, R., N. Dagan, and Y. Mahrer, 1986: "Evaluation, in Real Time, of the Actual Evapotranspiration Using a Numerical Model," *Proc. Agrotics 86, Automation and Robots for Agriculture*, 18–20 March 1986, Bordeaux, France.

Blackadar, A. K., 1978: "Modeling Pollutant Transfer During Daytime Convection," *Preprints, Fourth Symp. on Atmospheric Turbulence, Diffusion and Air Quality*, Reno, Amer. Meteorol. Soc., 443–447.

Blackadar, A. K., 1979: "High Resolution Models of the Planetary Boundary Layer," *Advances in Environmental Science and Engineering*, 1(1), J. Pfafflin and E. Ziegler (eds.), Gordon and Breach, 50–85.

Burk, S. D., 1977: "The Moist Boundary Layer with a Higher Order Turbulence Closure Model," *J. Atmos. Sci.* **34**, 629–638.

Burk, S. D., 1980: "Refractive Index Structure Parameters: Time Dependent Calculations Using a Numerical Boundary-Layer Model," *J. Appl. Meteorol.* **19**, 562–576.

Businger, J. A., J. C. Wyngaard, Y. Izumi, and E. F. Bradley, 1971: "Flux-Profile Relationships in the Atmospheric Surface Layer," *J. Atmos. Sci.* **28**, 181–189.

Carson, D. J., 1987: "An Introduction to the Parameterization of Land-Surface Processes: Part 1. Radiation and Turbulence," *Meteorological Magazine* **116**, 229–242.

Cionco, R. M., 1965: "A Mathematical Model for Air Flow in a Vegetative Canopy," *Appl. Meteorol.* **4**, 517.

Cionco, R. M., 1985: "Modeling Windfields and Surface-Layer Wind Profiles over Complex Terrain and Within Vegetative Canopies," *The Forest-Atmosphere Interaction*, B. A. Hutchinson and B. B. Hicks (eds.), D. Reidel Publishing Co., 501–520.

Clarke, R. H., A. J. Dyer, R. R. Brook, D. G. Reid, and A. J. Troup, 1971: *The Wangara Experiment: Boundary-Layer Data*, Commonwealth Scientific and Industrial Research Organization, Australia.

Deardorff, J. W., 1972: "Numerical Investigation of Neutral and Unstable Boundary Layers," *J. Atmos. Sci.* **29**, 91–115.

Deardorff, J. W., 1974: "Three-Dimensional Numerical Study of the Height and Mean Structure of a Heated Planetary Boundary Layer," *Bound. Layer Meteorol.* **7**, 81–106.

Deardorff, J. W., 1978: "Efficient Prediction of Ground Surface Temperature and Moisture, with Inclusion of a Layer of Vegetation," *J. Geophys. Res.* **83**(C4), 1889–1903.

Dyer, A. J., 1974: "A Review of Flux-Profile Relationships," *Bound. Layer Meteorol.* **7**, 363–372.

Gross, G., 1994: "Statistical Evaluation of the Mesoscale Model Results," *Mesoscale Modeling of the Atmosphere*, Meteorological Monograph No. 47, Amer. Meteorol. Soc., Boston, pp 137–156.

Hansen, F. V., 1993a: *Albedos*, Army Research Laboratory, ARL-TR-57.

Hansen, F. V., 1993b: *Surface Roughness Lengths*, Army Research Laboratory, ARL-TR-61.

Haurwitz, B., 1945: "Insolation in Relation to Cloudiness and Cloud Density," *J. Meteorol.* **2** (3), 154–166.

Huschke, R. E. (eds.), 1959: *Glossary of Meteorology*, Amer. Meteorol. Soc.

Kordova, L., Y. Mahrer, E. Rawitz, and M. Margolin, 1994: "Estimation of Actual Evapotranspiration by Utilizing Meteorological Numerical Models," *Proc. 21st Conf. Agric. Forest Meteorol.*, 7–11 March 1994, San Diego, CA, 283–286, Amer. Meteorol. Soc., Boston.

Mellor, G. L., and T. Yamada, 1974: "A Hierarchy of Turbulence Closure Models for Planetary Boundary Layers," *J. Atmos. Sci.* **31**, 1791–1806.

Meyers, T. P., and R. F. Dale, 1983: "Predicting Daily Insolation with Hourly Cloud Height and Coverage," *J. Clim. Appl. Meteorol.* **22**, 537–545.

McNider, R. T., and R. A. Pielke, 1981: "Diurnal Boundary-Layer Development over Sloping Terrain," *J. Atmos. Sci.* **38** (10), 2198–2212.

Monin, A. S., and A. M. Obukhov, 1954: "Basic Regularity in Turbulent Mixing in the Surface Layer of the Atmosphere," *Trans. Geophys. Inst. (Trudy) Acad. Sci. USSR* **24**, 163–187.

Naot, O., and Y. Mahrer, 1989: "Modeling Microclimate Environments: A Verification Study," *Bound. Layer Meteorol.* **46**, 333–354.

Noble, J. M., 1991: "Acoustic Propagation in the Atmosphere Using the Scanning Fast Field Program," *Proc. Battlefield Atmospherics Conf.*, 3–6 December, Fort Bliss, TX.

Noble, J. M., 1992: "The Importance of Ducting in Atmospheric Acoustics," *Proc. Battlefield Atmospherics Conf.*, 1–3 December, Fort Bliss, TX.

Noble, J. M., 1996: *User's Manual for the Microsoft Windows Scanning Fast Field Program (WSCAFFIP)*, Army Research Laboratory (in preparation).

Noble, J. M., and D. Marlin, 1995: *User's Manual for the Scanning Fast Field Program (SCAFFIP)*, Army Research Laboratory, ARL-TR-545.

O'Brien, J. J., 1970: "A Note on the Vertical Structure of the Eddy Exchange Coefficient in the Planetary Boundary Layer," *J. Atmos. Sci.* **27**, 1213–1215.

Pielke, R. A., and Y. Mahrer, 1975: "Representation of the Heated Planetary Boundary Layer in Mesoscale Models with Coarse Vertical Resolution," *J. Atmos. Sci.* **32** (12), 2288–2308.

Pierce, A. D., 1981: *Acoustics: An Introduction to Its Physical Principles and Applications*, McGraw-Hill, New York

Rachele, H., and A. Tunick, 1994: "Energy Balance Model for Imagery and Electromagnetic Propagation," *J. Appl. Meteorol.* **33**, 964–976.

Rachele, H., A. Tunick, and F. V. Hansen, 1995: "MARIAH—A Similarity Based Method for Determining Wind, Temperature, and Humidity Profile Structure in the Atmospheric Surface Layer," *J. Appl. Meteorol.* **34**, 1000–1005.

Rachele, H., A. Tunick, and F. V. Hansen, 1996a: "Reply," *J. Appl. Meteorol.* **35** (4), 613–614. (Reply to Arya, S. P., 1996: "Comments on 'MARIAH—A Similarity Based Method for Determining Wind, Temperature, and Humidity Profile Structure in the Atmospheric Surface Layer,'" *J. Appl. Meteorol.* **35** (4), 610–612.)

Rachele, H., A. Tunick, L. Kordova, and Y. Mahrer, 1996b: "A Radiation and Energy Balance Model for the Microscale-Surface-Layer Environment," *Proc. 22nd Conf. Agri. Forest Meteorol.*, 28 January–2 February, Atlanta, Amer. Meteorol. Soc., Boston.

Stenmark, E. B., and L. D. Drury, 1970: *Micrometeorological Field Data From Davis, California 1966–67, Runs Under Non-Advective Conditions*, U.S. Army Electronics Command, ECOM-6051, Atmospheric Sciences Laboratory, Fort Huachuca, AZ.

Woolf, H. M., 1968: *On the Computation of Solar Elevation Angles on the Determination of Sunrise and Sunset Times*, National Meteorological Center, Environmental Sciences Services Administration, Hillcrest Heights, MD.

Yamada, T., and G. L. Mellor, 1975: "A Simulation of the Wangara Atmospheric Boundary-Layer Data," *J. Atmos. Sci.* **32** (12), 2309–2329.

Zhang, D., and R. A. Anthes, 1982: "A High-Resolution Model of the Planetary Boundary Layer—Sensitivity Tests and Comparisons with SESAME-79 Data," *J. Appl. Meteorol.* **21**, 1594–1609.

Distribution

Admnstr
Defns Techl Info Ctr
Attn DTIC-OCP
8725 John J Kingman Rd Ste 0944
FT Belvoir VA 22060-6218

Mil Asst for Env Sci
Ofc of the Undersec of Defns for
  Rsrch & Engrg R&AT E LS
Pentagon Rm 3D129
Washington DC 20301-3080

Ofc of the Dir Rsrch and Engrg
Attn R Menz
Pentagon Rm 3E1089
Washington DC 20301-3080

Ofc of the Secy of Defns
Attn ODDRE (R&AT) G Singley
Attn ODDRE (R&AT) S Gontarek
The Pentagon
Washington DC 20301-3080

OSD
Attn OUSD(A&T)/ODDDR&E(R) J Lupo
Washington DC 20301-7100

ARL Chemical Biology Nuc Effects Div
Attn AMSRL-SL-CO
Aberdeen Proving Ground MD 21005-5423

Army Communications Elec Ctr for EW RSTA
Attn AMSEL-EW-D
FT Monmouth NJ 07703-5303

Army Corps of Engrs
Engr Topographics Lab
Attn ETL-GS-LB
FT Belvoir VA 22060

Army Dugway Proving Ground
Attn STEDP 3
Attn STEDP-MT-DA-L-3
Attn STEDP-MT-M Biltoft
Attn STEDP-MT-M Bowers
Dugway UT 84022-5000

Army Field Artillery School
Attn ATSF-TSM-TA
FT Sill OK 73503-5000

Army Foreign Sci Tech Ctr
Attn CM
220 7th Stret NE
Charlottesville VA 22901-5396

Army Infantry
Attn ATSH-CD-CS-OR E Dutoit
FT Benning GA 30905-5090

Army Materiel Sys Analysis Activity
Attn AMXSY-AT Campbell
Attn AMXSY-CR Marchetti
Attn AMXSY-CS Bradley
Aberdeen Proving Ground MD 21005-5071

Army Missile Cmnd
Attn AMSMI-RD-AC-AD Peterson
Redstone Arsenal AL 35898-5242

Army Missile Cmnd
Attn AMSMI-RD-DE-SE G Lill Jr
Redstone Arsenal AL 35898-5245

Army Missile Cmnd
Attn AMSMI-RD-AS-SS B Williams
Attn AMSMI-RD-AS-SS H F Anderson
Redstone Arsenal AL 35898-5253

Army Rsrch Ofc
Attn AMXRO-GS Bach
PO Box 12211
Research Triangle Park NC 27709

Army Strat Defns Cmnd
Attn CSSD-SL-L Lilly
PO Box 1500
Huntsville AL 35807-3801

Army TACOM-ARDEC
Attn AMSTA-AR-WEL-TL
Bldg 59 Phillips Rd
Picatinny Arsenal NJ 07806-5000

CECOM
Attn PM GPS COL S Young
FT Monmouth NJ 07703

CECOM RDEC Elect System Div Dir
Attn J Niemela
FT Monmouth NJ 07703

25

Distribution

CECOM Sp & Terrestrial Commctn Div
Attn AMSEL-RD-ST-MC-M H Soicher
FT Monmouth NJ 07703-5203

Div of Atmos Sci Natl Sci Foundation
Attn Bierly
1800 G Stret NW
Washington DC 20550

Dpty Assist Secy for Rsrch & Techl
Attn SARD-TR R Chait Rm 3E476
Attn SARD-TT D Chait
Attn SARD-TT F Milton Rm 3E479
Attn SARD-TT K Kominos
Attn SARD-TT R Reisman
Attn SARD-TT T Killion
The Pentagon
Washington DC 20301-0103

Hdqtrs Dept of the Army
Attn DAMO-FDT D Schmidt
400 Army Pentagon Rm 3C514
Washington DC 20301-0460

Hdqtrs Dept of the Army
Attn DAMI-POI
Washington DC 20301-1067

Kwajalein Missile Range
Attn Meteorologist in Charge
PO Box 57
APO San Francisco CA 96555

Logistics Ctr
Attn ATCL-CE
FT Lee VA 23801-6000

Natl Security Agency
Attn W21   Longbothum
9800 Savage Rd
FT George G Meade MD 20755-6000

Naval Air Dev Ctr
Attn Code 5012 A Salik
Warminister PA 18974

Pac Mis Test Ctr Geophysics Div
Attn Code 3250   Battalino
Point Mugu CA 93042-5000

Science & Technology
101 Research Dr
Hampton VA 23666-1340

US Army Aviation Ctr
Attn ATZQ-D-MA   Heath
FT Rucker AL 36362

US Army CECRL
Attn CECRL-RG   Boyne
Hanover NH 03755-1290

US Army Chem School
Attn ATZN-CM-CC   Barnes
FT McClellan AL 36205-5020

US Army Combined Arms Combat
Attn ATZL-CAW
FT Leavenworth KS 66027-5300

US Army Field Artillery Schl
Attn ATSF-F-FD   Gullion
Attn ATSF-TSM-TA   Taylor
FT Sill OK 73503-5600

US Army Matl Cmnd
Dpty CG for RDE Hdqtrs
Attn AMCRD BG Beauchamp
5001 Eisenhower Ave
Alexandria VA 22333-0001

US Army Matl Cmnd
Prin Dpty for Acquisition Hdqrts
Attn AMCDCG-A D Adams
5001 Eisenhower Ave
Alexandria VA 22333-0001

US Army Matl Cmnd
Prin Dpty for Techlgy Hdqrts
Attn AMCDCG-T M Fisette
5001 Eisenhower Ave
Alexandria VA 22333-0001

US Army Mis Cmnd (USAMICOM)
Attn AMSMI-RD-CS-R Documents
Redstone Arsenal AL 35898-5400

US Army Nuclear & Chem Agency
Attn MONA-ZB
Bldg 2073
Springfield VA 22150-3198

Distribution

US Army OEC
Attn CSTE-EFS
Park Center IV 4501 Ford Ave
Alexandria VA 22302-1458

US Army Spc Instit
Attn ATZI-SI
Attn ATZL-SI-D
FT Leavenworth KS 66027-5300

US Army Spc Technology Rsrch Ofc
Attn Brathwaite
5321 Riggs Rd
Gaithersburg MD 20882

US Army Topo Engrg Ctr
Attn CETEC-ZC
FT Belvoir VA 22060-5546

US Army TRADOC Anlys Cmnd—WSMR
Attn ATRC-WSS-R
White Sands Missile Range NM 88002

US Army White Sands Missile Range
Attn STEWS-IM-IT Techl Lib Br
White Sands Missile Range NM 88002-5501

US Army Intel Ctr and FT Huachuca
Attn ATSI-CDC-C Colanto
FT Huachuca AZ 85613-7000

US Military Academy
Dept of Mathematical Sci
Attn MAJ D Engen
West Point NY 10996

USAASA
Attn MOAS-AI W Parron
9325 Gunston Rd Ste N319
FT Belvoir VA 22060-5582

USACRREL
Attn CEREL-GP R Detsch
72 Lyme Rd
Hanover NH 03755-1290

USATRADOC
Attn ATCD-FA
FT Monroe VA 23651-5170

Nav Air War Cen Wpn Div
Attn CMD 420000D C0245 A Shlanta
1 Admin Cir
China Lake CA 93555-6001

Nav Ocean Sys Ctr
Attn Code 54 Richter
San Diego CA 92152-5000

Nav Rsrch Lab
Attn Code 4110 Ruhnke
Washington DC 20375-5000

Nav Surface Warfare Ctr
Attn Code B07 J Pennella
17320 Dahlgren Rd Bldg 1470 Rm 1101
Dahlgren VA 22448-5100

Nav Weapons Ctr
Attn Code 3331 Shlanta
China Lake CA 93555

Naval Surface Weapons Ctr
Attn Code G63
Dahlgren VA 22448-5000

OIC-NAVSWC
Attn Code E-232 Techl Lib
Silver Spring MD 20903-5000

Spc & Nav Warfare Sys Cmnd
Attn PMW-145-1G
Washgton DC 20362-5100

AFMC DOW
Wright Patterson AFB OH 45433-5000

Air Weather Service
Attn TechL Lib FL4414 3
Scott AFB IL 62225-5458

Dept of the Air Force
Attn OL A 2D Weather squad Mac
Holloman AFB NM 88330-5000

GPS Joint Prog Ofc Dir
Attn COL J Clay
2435 Vela Way Ste 1613
Los Angeles AFB CA 90245-5500

Distribution

Hdqtrs AWS DOO 1
Scott AFB IL 62225-5008

Phillips Lab Atmos Sci Div
Geophsics Directorate
Attn McClatchey
Hanscom AFB MA 01731-5000

Phillips Laboratory
Attn PL/LYP 3
Attn PL/LYP Chisholm
Attn PL/WE
Kirtland AFB NM 87118-6008

Special Assist to the Wing Cmndr
Attn 50SW/CCX Capt P H Bernstein
300 O'Malley Ave Ste 20
Falcon AFB CO 80912-3020

TAC/DOWP
Langley AFB VA 23665-5524

USAF Rome Lab Tech
Attn Corridor W Ste 262 RL SUL
26 Electr Pkwy Bldg 106
Griffiss AFB NY 13441-4514

USAFETAC DNE
Attn Glauber
Scott AFB IL 62225-5008

DARPA
Attn B Kaspar
Attn L Stotts
3701 N Fairfax Dr
Arlington VA 22203-1714

Nasa Marshal Space Flt Ctr
Atmospheric Sciences Div
Attn E501 Fichtl
Huntsville AL 35802

Nasa Spct Flt Ctr Atmospheric Sciences Div
Attn Code ED 41 1
Attn Code ED-41
Huntsville AL 35812

ARL Electromag Group
Attn Campus Mail Code F0250 A Tucker
University of Texas
Austin TX 78712

Colorado State Univ
Dept of Atmospheric Sci
Attn R A Pielke
FT Collins CO 80523

Cornell Univ School of Civil & Env
Attn W H Brutsaert
Hollister Hall
Ithica NY 14853-3501

Florida State Univ Dept of Meteorology
Attn E A Smith
Tallahassee FL 32306

Iowa State Univ
Attn E S Takle
Attn R Arritt
312 Curtiss Hall
Ames IA 50011

Iowa State Univ
Attn M Segal
Attn S E Taylor
2104 Agronomy Hall
Ames IA 50011-1010

Michigan State Univ Dept of Crop & Soil Sci
Attn J Ritchie
8570 Plant & Soil Sciences Bldg
East Lansing MI 48824-1325

Penn State Univ Dept of Meteorology
Attn D Thompsom
503 Walker Bldg
University Park PA 16802

Rutgers Univ-Cook
Campus Envir & Natl Resources Bldg
Attn R Avissar
New Brunswick NJ 08903

Univ of California at Davis
Dept of Air, Land, & Water Resources
Attn R H Shaw
Davis CA 95616

Univ of Connecticut
Dept of Renewable Natural Resources
Attn D R Miller
1376 Storrs Rd
Storrs CT 06269-4087

Distribution

Univ of Nebraska
Dept of Agrcltl Meteorology
Attn S B Verma
Lincoln NE 68583-0728

Univ of Alabama at Huntsville Rsrch Instit
Attn R T Mcnider
Huntsville AL 35899

University of Kansas
Dept of Physics & Astronomy
Attn J R Eagleman
Lawrence KS 66045

Washington State Univ
Dept of Agronomy & Soils
Attn G S Campbell
Pullman WA 99163

Agrclt Rsrch Svc Conserve & Prodn Rsrch Lab
Attn A D Schneider
Attn S R Evett
Attn T A Howell
PO Drawer 10
Bushland TX 79012

Dean RMD
Attn Gomez
Washington DC 20314

Dept of Commerce Ctr
Mountain Administration
Attn Spprt Ctr Library R51
325 S Broadway
Boulder CO 80303

Natl Ctr for Atmospheric Research
Attn NCAR Library Serials
Attn T W Horst
Attn S P Oncley
PO Box 3000
Boulder CO 80307-3000

NCSU
Attn J Davis
PO Box 8208
Raleigh NC 27650-8208

Northrup Corp Elect Sys Div
Attn Tooley
2301 W 120th Stret Box 5032
Hawthrone CA 90251-5032

NTIA ITS S3
Attn H J Liebe
325 S Broadway
Boulder CO 80303

Pacific Missile Test Ctr Geophysics Div
Attn Code 3250
Point Mugu CA 93042-5000

Raytheon Company Equip div
Attn Sonnenschein
528 Boston Post Rd MS 1K9
Sudbury MA 01776

Sigma Rsrch Corp
Attn S R Hanna
544 Hill Rd
Boxborough MA 01719

USDA Agrcltl Rsrch Svc
Attn W PKustas Kustas
BARC0WEST Bldg 265
Beltsville MD 20705

USDA Agrcltl Rsrch Svc
Attn R D Jackson
Attn S B Idso
4331 E Broadway Rd
Phoenix AZ 85040

USDA Forest Svc Rocky Mtn Frst & Range
  Exprmnt Sta
Attn K F Zeller
240 W Prospect Stret
FT Collins CO 80526

US Army Rsrch Lab
Attn DRXRO-GS   Flood
PO Box 12211
Research Triangle Park NC 27009

US Army Rsrch Lab
Attn AMSRL-IS-EA J Harris
Attn AMSRL-IS-EW D Hoock
Attn AMSRL-BE-A   Rubio
Attn AMSRL-BE-A   Seagraves
Battlefield Envir Dir
White Sands Missile Range NM 88002-5001

Distribution

US Army Rsrch Lab
Attn AMSRL-BE D R Veazey
Attn AMSRL-CI-LL Techl Lib (3 copies)
Attn AMSRL-CS-AL-TA Mail & Records
  Mgmt
Attn AMSRL-CS-AL-TP Techl Pub (3 copies)
Attn AMSRL-IS-CS J D Gantt
Attn AMSRL-IS-E   Brown

US Army Rsrch Lab (cont'd)
Attn AMSRL-IS-EE A D Tunick
  (15 copies)
Attn AMSRL-IS-EE D Garvey
Attn AMSRL-IS-EE R Meyers
Attn AMSRL-SE-EE Z G Sztankay
Adelphi MD 20783-1197

REPORT DOCUMENTATION PAGE

Form Approved
OMB No. 0704-0188

1. AGENCY USE ONLY *(Leave blank)*	2. REPORT DATE November 1997	3. REPORT TYPE AND DATES COVERED Final, November 1995–June 1997	

4. TITLE AND SUBTITLE

Evaluation of an Atmospheric Microclimate Model

5. FUNDING NUMBERS

DA PR: B53A
PE: P61102

6. AUTHOR(S)

Arnold D. Tunick

7. PERFORMING ORGANIZATION NAME(S) AND ADDRESS(ES)

U.S. Army Research Laboratory
Attn: AMSRL-IS-EE
2800 Powder Mill Road
Adelphi, MD 20783-1197

8. PERFORMING ORGANIZATION REPORT NUMBER

ARL-TR-1459

9. SPONSORING/MONITORING AGENCY NAME(S) AND ADDRESS(ES)

U.S. Army Research Laboratory
2800 Powder Mill Road
Adelphi, MD 20783-1197

10. SPONSORING/MONITORING AGENCY REPORT NUMBER

11. SUPPLEMENTARY NOTES

AMS code: 611102.53A11
ARL PR: 7FEJ60

12a. DISTRIBUTION/AVAILABILITY STATEMENT

Approved for public release; distribution unlimited.

12b. DISTRIBUTION CODE

13. ABSTRACT *(Maximum 200 words)*

Micrometeorological field data were used in an effort to evaluate an atmospheric microclimate model, specifically, to determine if we can forecast one-dimensional profiles of the atmospheric boundary layer sufficiently well that the corresponding outdoor acoustic field can be reliably calculated.

A soil–plant–atmosphere model was exercised with two sets of experimental data. The model was used to calculate the surface energy budget and to derive meteorological profiles for the overlying boundary layer; both of these were compared to field data. These modeled results were also used to derive outdoor sound-speed profiles and were used as input to a short-range acoustic propagation numerical code.

14. SUBJECT TERMS

Microclimate, atmospheric acoustics, atmospheric boundary layer, surface energy budget

15. NUMBER OF PAGES
36

16. PRICE CODE

17. SECURITY CLASSIFICATION OF REPORT Unclassified	18. SECURITY CLASSIFICATION OF THIS PAGE Unclassified	19. SECURITY CLASSIFICATION OF ABSTRACT Unclassified	20. LIMITATION OF ABSTRACT UL